LEVEL II

12

NSWC/WOL TR 77-123

AD A064908

DDC FILE COPY

EXPLOSIVE OPTIMIZATION FOR A FORTY-TWO DEGREE CONICAL SHAPED CHARGE

BY J. P. COUGHLIN

RESEARCH AND TECHNOLOGY DEPARTMENT

28 NOVEMBER 1978

Approved for public release, distribution unlimited.

DDC
RECEIVED
FEB 26 1979
D

NAVAL SURFACE WEAPONS CENTER

Dahlgren, Virginia 22448 • Silver Spring, Maryland 20910

79 02 21 016

UNCLASSIFIED

SECURITY CLASSIFICATION OF THIS PAGE *(When Data Entered)*

REPORT DOCUMENTATION PAGE	READ INSTRUCTIONS BEFORE COMPLETING FORM
1. REPORT NUMBER: NSWC/WOL/TR-77-123	2. GOVT ACCESSION NO. / 3. RECIPIENT'S CATALOG NUMBER
4. TITLE (and Subtitle): EXPLOSIVE OPTIMIZATION FOR A FORTY-TWO DEGREE CONICAL SHAPED CHARGE,	5. TYPE OF REPORT & PERIOD COVERED: Final Report,
	6. PERFORMING ORG. REPORT NUMBER
7. AUTHOR(s): J. P. Coughlin	8. CONTRACT OR GRANT NUMBER(s)
9. PERFORMING ORGANIZATION NAME AND ADDRESS: Naval Surface Weapons Center, White Oak, Silver Spring, Maryland 20910	10. PROGRAM ELEMENT, PROJECT, TASK AREA & WORK UNIT NUMBERS: 63610N; S0199, S0199-111, CR16CA
11. CONTROLLING OFFICE NAME AND ADDRESS	12. REPORT DATE: 28 November 1978
	13. NUMBER OF PAGES: 38
14. MONITORING AGENCY NAME & ADDRESS *(if different from Controlling Office)*: 39 p.	15. SECURITY CLASS. *(of this report)*: Unclassified
	15a. DECLASSIFICATION/DOWNGRADING SCHEDULE

16. DISTRIBUTION STATEMENT *(of this Report)*

Approved for Public Release, distribution unlimited.

17. DISTRIBUTION STATEMENT *(of the abstract entered in Block 20, if different from Report)*

18. SUPPLEMENTARY NOTES

19. KEY WORDS *(Continue on reverse side if necessary and identify by block number)*

Shaped Charge
Jet
Hydrocalculations
Explosives
Numerical Analysis

20. ABSTRACT *(Continue on reverse side if necessary and identify by block number)*

Computational studies on the jet from a forty-two degree conical liner are reported. Three different modes of initiation were studied with a view to predicting the best jet. The explosive parameters were varied systematically with a view to determining the effects of each parameter on the jet formed.

DD FORM 1 JAN 73 1473 EDITION OF 1 NOV 65 IS OBSOLETE
S/N 0102-LF-014-6601

391 596

UNCLASSIFIED

SECURITY CLASSIFICATION OF THIS PAGE *(When Data Entered)*

SUMMARY

Computational studies on the jet from a forty-two degree conical liner are reported. Three different modes of initiation were studied with a view to predicting the best jet. The explosive parameters were varied systematically with a view to determining the effects of each parameter on the jet formed.

Julius W. Enig

JULIUS W. ENIG
By direction

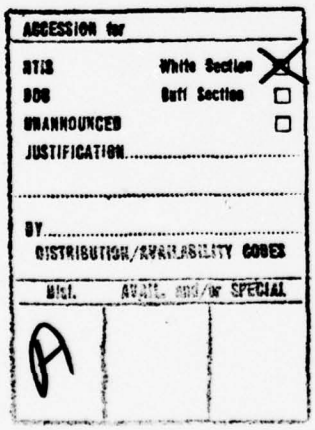

TABLE OF CONTENTS

EXPLOSIVE OPTIMIZATION FOR A FORTY-TWO DEGREE CONICAL SHAPED CHARGE

INTRODUCTION

In optimizing the performance of a forty-two degree conical shaped charge, two big factors are the explosive chosen and the mode of initiation for the explosive. The effects of both of these variables can be studied computationally and that study forms the subject matter of this report.

The baseline design considered for this study was the forty-two degree cone shown in Figure 1. (All dimensions are in centimeters). The liner is made of copper and, for computational purposes, elastic-plastic effects are ignored and the purely hydrodynamic Tillotson equation-of-state is used[1]. The explosive is pentolite and the reaction products are treated by a gamma law equation-of-state. The explosive column is short, being only about 3 centimeters (0.4 cone diameters) long.

The computations were carried out using the (two dimensional) BRLSC code developed by Science, Systems and Software Corporation from their earlier HELP code for the specific purpose of computing shaped charges[1].

In Part I, three different modes of initiation are studied: A point detonation at the point, P, on the symmetry axis (see Figure 1); a plane wave detonation in the plane of the points, P and Q, (end face of the explosive column), and a circumferential initiation in the ring obtained by rotating Q around the symmetry axis.

In Part II, three different hypothetical explosives were used. The baseline calculation was the plane wave initiated cone using pentolite as the explosive. By varying the value of gamma by 10% a new (hypothetical) explosive was obtained. The results of this calculation are compared to the baseline calculation. Similarly, two more explosives are obtained by varying the detonation energy and the loading density by 10%. While these explosives correspond to no real explosive, they each serve to indicate the effect of the varied parameter on the jet produced.

PART I - EFFECTS OF DIFFERENT MODES OF INITIATION

As mentioned above, three different modes of initiation are considered--point initiation, plane wave initiation, and

circumferential initiation. In each case a detonation wave is formed and travels down the explosive until it collides with the liner. Upon collision, a reflected shock arises on the locus of the intersection of the detonation wave and the liner. At 10 μsec after initiation, the pressures in the explosive are as shown in the pressure maps of Figures 2, 3, and 4. These maps are based on an Eulerian grid which divides the space of interest into fixed cells. For each of these cells a pressure is calculated. In order to present the results visually, a letter is assigned to various pressure ranges (see Figures 2, 3, and 4) and the letter appearing in the cell indicates the range to which the cell pressure belongs. The pressure ranges corresponding to each letter are shown at the bottom of the figure. (The ranges are not the same for all three figures).

The point initiated case is shown in Figure 2. The detonation wave forms a circular arc and there is no real sign of a reflected wave. This may be explained as follows. In Figure 5, the detonation originates at the point P and reaches the apex of the conical liner at the point, O. At some later time, the detonation front will be a circular arc centered at P and intersecting the wall at the point, Q. The front will be perpendicular to the radius, PQ, and make an angle, ψ_i, with the wall. The base angle of the cone is $\alpha=21°$. From the law of sines:

$$T \csc \phi = D^*t \csc (180-\alpha)$$

$$\sin \phi = T \sin\alpha / D^*t$$

And, from the figure, $\cos \psi_i = \sin (90-\psi_i) = \sin \phi$:

$$\cos \psi_i = T \sin\alpha / D^*t$$

Using the values: D (detonation velocity) = 0.736 cm/μsec, t (time) = 10 μsec, T (see Figure 5) = 2.563 cm, and $\alpha = 21^\circ$ we see that ψ_i must be 82.8°. Using this value of ψ_i and the detonation properties of pentolite, the coefficients of the cubic equation of Appendix A can be calculated, and the resulting equation has no positive real roots. Consequently, there is no solution to the regular reflection problem. The reflected shock must be a Mach reflection which could easily be obscured by the relief waves from the sides (the low pressure regions on the right of Figure 2).

In the plane wave initiated case (see Figure 3) the detonation front is a straight, horizontal line except near the edges of the explosive where the relief wave makes itself felt. The reflected wave is found by moving horizontally across the figure. As we move from right to left, the pressure rises and then falls off. The pressure maxima (found in the shaded boxes of Figure 3) approximately locate the reflected shock. Near the liner, the reflected shock makes an angle of nearly 45° with the detonation

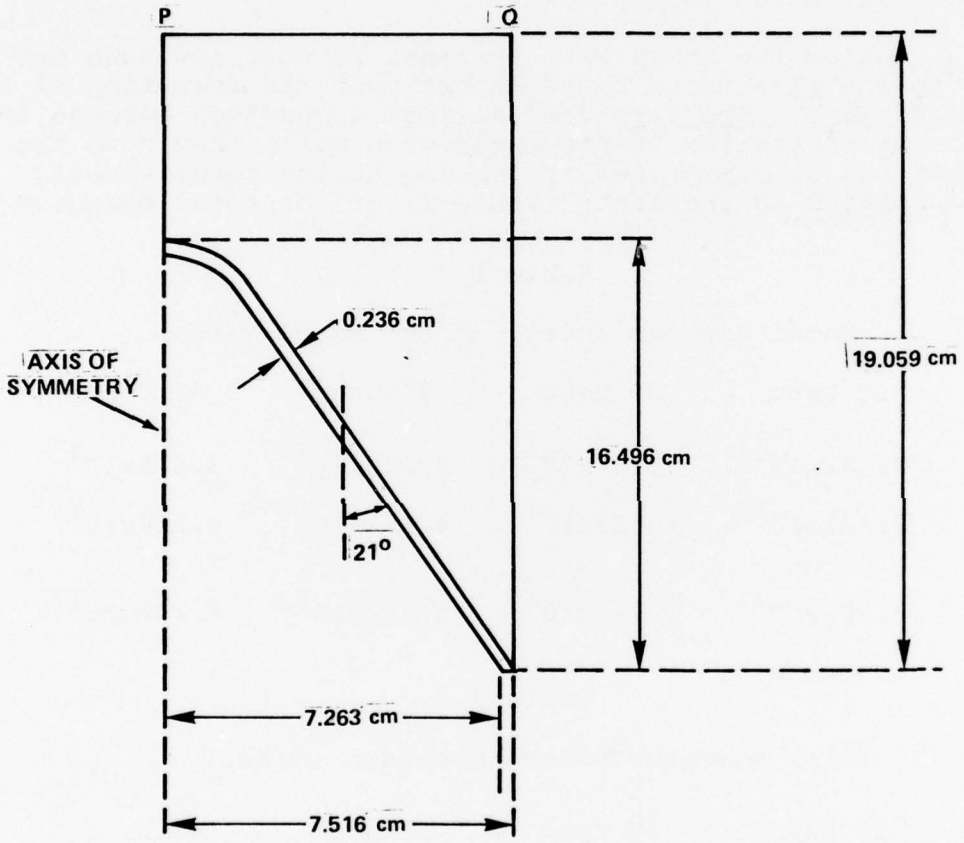

FIG. 1 CROSS SECTION OF THE 42° CONE, SHOWING THE DIMENSIONS

70 02 21 016

front and then turns to a nearly vertical position (90° to the front). The angle of incidence is 90°-21° = 69° and the calculation of Appendix A shows that there are no solutions to the regular reflection problem. The shock system we are looking at is a Mach configuration somewhat obscured by the smearing out of the detonation wave over three zones.

In the circumferentially initiated case (Figure 4), the shock is incident upon the liner head-on, and the reflection corresponds to a normal reflection fairly well.

Having studied the shock wave systems, we must now turn our attention to the effects of these shocks upon the formation of the shaped charge jets. The first and easiest comparison between the three modes of initiation is the speed with which they move the metal. This can be summarized by looking at the total kinetic energy transmitted to the liner (Table 1) or the total momentum (Table 2).

Table 1

Total Kinetic Energy of the Metal (ergs)

	10 μsec	20 μsec	30 μsec	40 μsec
Point	7.642×10^{11}	7.132×10^{12}	2.820×10^{13}	3.576×10^{13}
Plane	2.131×10^{12}	1.623×10^{13}	4.178×10^{13}	4.246×10^{13}
Circum-ferential	3.507×10^{11}	1.725×10^{13}	3.924×10^{13}	4.142×10^{13}

Table 2

Total Momentum of the Metal (gm cm/sec)

	10 μsec	20 μsec	30 μsec	40 μsec
Point	8.699×10^{6}	5.098×10^{7}	1.469×10^{8}	1.907×10^{8}
Plane	1.617×10^{7}	9.010×10^{7}	1.980×10^{8}	2.306×10^{8}
Circum-ferential	3.009×10^{6}	8.890×10^{7}	1.888×10^{8}	2.228×10^{8}

These values are plotted in Figures 6 and 7. The most obvious result is the inferiority of point detonation as a means of initiating shaped charges. The other two modes of initiation are roughly comparable, with the plane initiation having a slight advantage. To differentiate further, we turn our attention to the jet formed. Figures 8, 9, and 10 show the position of the metal after 40 μsec. As can be seen from Figures 8, 9, and 10,

in all three cases, at 40 μseconds, the liner is divided into three parts--a slug at the top, the undeformed liner on the right (which is approximately in its original shape) and the jet at the bottom which is separating from the other two. In each figure a horizontal line may be drawn which separates the jet below from the slug above. This line is drawn where the surface of the metal turns sharply to the side and begins to move back downward. All the cells in the grid below this line belong to the jet, and all those above do not. Taking the values of mass, m_{ij}, and velocity, v_{ij}, for all such cells and forming the sums: Σm_{ij}, $\Sigma m_{ij}\ v_{ij}$, and $\Sigma\ 1/2\ m_{ij}\ v_{ij}^2$, gives the total mass, momentum, and energy in the jet. The results for the three different modes of initiation are summarized in Table 3 for the jet at 30 μseconds, and in Table 4 for the jet at 40 μseconds.

Table 3

Properties of the Jet (30 μsec.)

	Jet Mass gm	Momentum gm cm/sec	Kinetic Energy ergs
Point	6.028	0.3845×10^7	1.228×10^{12}
Plane	15.570	1.111×10^7	3.996×10^{12}
Circum-ferential	16.458	1.292×10^7	5.117×10^{12}

In Tables 1 and 2 it is seen that circumferential initiation and plane wave initiation are approximately equal in terms of the momentum and kinetic energy given the liner. In Table 3, it is seen that circumferential initiation puts more mass, momentum, and energy in the jet. Since the jet is the penetrating mechanism, circumferential initiation is clearly superior. The superiority is even more evident at 40 μseconds as seen in Table 4:

Table 4

Properties of the Jet (40 μsec.)

	Jet Mass gm	Momentum gm cm/sec	Kinetic Energy ergs
Point	14.91	1.103×10^7	4.085×10^{12}
Plane	29.23	2.144×10^7	7.881×10^{12}
Circum-ferential	34.52	2.533×10^7	9.380×10^{12}

The values at 40 μseconds were used to test the sensitivity of the results to the exact location of the horizontal line which separates the jet from the rest of the metal. Accordingly, the sums used to define jet mass, momentum, and kinetic energy were extended to include one extra row of zones. The revised figures are in Table 5.

Table 5

Properties of the Jet at 40 μseconds--Extra Zones Included

	Jet Mass	Momentum	Kinetic Energy
	gm	gm cm/sec	ergs
Point Detonation	22.89	1.587×10^{7}	5.571×10^{12}
Plane Wave	41.43	2.848×10^{7}	9.935×10^{12}
Circum-ferential	45.69	3.171×10^{7}	11.20×10^{12}

If the second row of Table 4 was divided by the first, the result is about 1.9 for each column indicating a 90% improvement over the point detonation mode. The same operation on Table 5 gives 1.8. The difference is not believed to be significant. For the quotient of row 3 by row 2, Table 4 gives 1.2 and Table 5 gives 1.1. Again, the difference is not believed to be significant and the results do not seem to depend critically on the location of the horizontal line mentioned above. Even more significantly, the near constancy of the ratio seems to indicate that an increase in mass of the jet increases the other quantities proportionally. The distribution of pressures and velocities in the jet at 30 μseconds is shown in Figure 11 for the point initiated charge, the plane wave initiated charge, and the circumferential initiated charge. The circumferentially initiated charge has produced a fully developed jet, because, as we move to the right in Figure 11 (toward the jet tip), the velocity increases monotonically and the pressure falls to zero almost immediately. The plane wave initiated jet is not yet developed because the velocity, though increasing rapidly at first, peaks and declines somewhat. The pressures (shown below) are still substantial and further accelerations will take place. The point initiated charge produces the worst jet of all with the velocities peaking and declining sharply while the pressures are still high. This jet obviously needs more time to develop.

The situation at 40 μseconds is shown in Figure 12. The circumferentially initiated jet has not changed qualitatively. The velocity is still increasing as we move out on the jet and the pressure falls to zero almost immediately. The plane wave initiated jet shows signs of further development. The velocity no longer peaks and falls off sharply, but falls off more gradually. Although

the velocity peak has risen, the tip velocity is within 98.11% of the peak velocity at 40 μseconds as opposed to only 96.64% at 30 μseconds. The pressures also have fallen off sharply. The point initiated jet seems to have undergone very little further development. The velocity gradient is still wrong and the pressures remain high even up to the tip of the jet. In fact, the situation seems to be getting worse, since the tip velocity is further away from the peak velocity at 40 μseconds than at 30 μseconds.

From these results, we can conclude that, for the charge configuration considered here, the circumferential mode of initiation is clearly the superior mode. The point detonation mode, although convenient, is a poor way to detonate this charge. (The point initiated case is not discussed in the following).

The stability of the remaining two cases is now examined. It is known that a jet will be radially unstable and show early signs of breakup if the velocity with which it enters the stagnation point is supersonic[2]. The stagnation point is easily located since it is in the zone (on the axis) with the highest pressure (see Figure 13). The sound speed at this point can be computed from the (Tillotson) equation-of-state by the relation:

$$c^2 = \frac{\partial f}{\partial \rho} + \frac{\partial f}{\partial I} p/\rho^2$$

where f is the Tillotson function[1], I is the internal energy, ρ the density, p the pressure and c the sound speed. The difference in velocity between the jet tip and the velocity at this point (V_o) must be less than the sound speed. For the plane wave initiated charge, the sound speed at the stagnation point is found to be .80 cm/μsec. The jet emerges with a velocity of .83 cm/μsec and, using the Birkhoff, Taylor, Pugh, and MacDougall theory[3], the collapse velocity, V_o (see Figure 13), can be found from:

$$\sin \frac{\beta-\alpha}{2} = \frac{V_o}{2D} \cos \alpha$$

$$V_j = V_o \csc(\beta/2) \cos (\alpha/2)$$

Solving the second of these equations for β, and eliminating β from the first, yields

$$\frac{V_o}{2D} \cos \alpha = \frac{V_o}{V_j} \cos^2 (\alpha/2) - \sin (\alpha/2) \left[1 - \frac{V_o^2}{V_j^2} \cos^2 (\alpha/2)\right]^{1/2}$$

Solving for V_o:

$$V_o = \frac{\sin(\alpha/2)}{\left[\left\{\frac{\cos\alpha}{2U} - \frac{\cos^2(\alpha/2)}{V_j}\right\}^2 + \frac{\sin^2\alpha}{4V_j^2}\right]^{1/2}}$$

Now $\alpha = 21^o$, $V_j = 0.83$ cm/μsec, and D=0.736 cm/μsec, so that $V_o = 0.32$ cm/μsec, which is definitely less than the sound speed computed for the stagnation zone. For the circumferentially initiated charge, the jet tip velocity, V_j, is 1.0 cm/μsecond. The calculated sound velocity at the stagnation reqion is 0.80 cm/μsec and, from the above formula, $V_o = 0.48$ cm/μsec. This case is also stable.

We can conclude that circumferential initiation is a superior mode of initiation producing a better and faster jet than either of the other two modes of initiation.

PART II - VARIATION OF EXPLOSIVE PARAMETERS

The question of the effects of initiation on the jet produced is part of a broader question of the effects of different explosives on jet production. More specifically, the explosive can be characterized by its loading density, ρ_o; and its chemical energy, Q (or E_{CJ}, the energy of the explosion products at the Chapman-Jouguet state), and by the parameter, γ, that occurs in the equation-of-state for the reaction products:

$$p = (\gamma-1)\, E/\rho.$$

A systematic study of the importance of these three parameters was undertaken to determine the effects of varying each of them upon the jet produced. The plane wave initiated charge (of Part I) with pentolite explosive was chosen as a standard for comparison. This will be referred to as the baseline design. Three more explosives were obtained by increasing each of the parameters mentioned above by 10%. They are called the density varied explosive ($\Delta\rho$), the energy varied explosive (ΔE), and the gamma varied explosive ($\Delta\gamma$). The jets that each of these explosives produces are named for the corresponding explosive.

The results of the calculation can be summarized, first with regard to the total energy and momentum (communicated) to the metal, by Tables 6 and 7; and with regard to the jet properties by Table 8.

Table 6

Total Kinetic Energy of the Metal vs. Time

	Kinetic Energy (ergs)			
Time	Baseline	ΔE	$\Delta\gamma$	$\Delta\rho$
10 μseconds	0.2131×10^{13}	0.2058×10^{13}	0.266×10^{13}	0.239×10^{13}
20 μseconds	1.623×10^{13}	1.887×10^{13}	1.966×10^{13}	1.783×10^{13}
30 μseconds	4.178×10^{13}	4.775×10^{13}	4.787×10^{13}	4.514×10^{13}
40 μseconds	4.246×10^{13}	4.693×10^{13}	4.539×10^{13}	4.599×10^{13}

Table 7

Total Momentum of the Metal vs. Time

	Momentum (gm cm/sec)			
Time	Baseline	ΔE	$\Delta\gamma$	$\Delta\rho$
10 μseconds	0.1617×10^{8}	0.1768×10^{8}	0.1847×10^{8}	0.1734×10^{8}
20 μseconds	0.9010×10^{8}	0.9919×10^{8}	1.014×10^{8}	0.9574×10^{8}
30 μseconds	1.980×10^{8}	2.150×10^{8}	2.129×10^{8}	2.091×10^{8}
40 μseconds	2.306×10^{8}	2.471×10^{8}	2.410×10^{8}	2.435×10^{8}

These results are displayed in Figures 14 and 15. All three of the varied explosives produce a greater kinetic energy and momentum in the liner than does the original pentolite, but there is little to choose from between the three of them. Accordingly, we turn to Table 8 to compare the jets produced:

Table 8

Properties of the Jet at 40 μseconds

	Mass	Momentum	Kinetic Energy
	gm	gm cm/sec	ergs
Baseline	29.23	2.144×10^{7}	7.881×10^{12}
ΔE	31.26	2.372×10^{7}	9.024×10^{12}
$\Delta \gamma$	30.43	2.336×10^{7}	8.995×10^{12}
$\Delta \rho$	36.63	2.683×10^{7}	9.863×10^{12}

From Table 8 it is clear that an increase of density is far and away the most effective way to increase jet performance. An increase in explosive energy is next and an increase in gamma is last, although not very far behind. The pressures and velocities at 30 μseconds are plotted in Figure 16 and the values at 40 μseconds are plotted in Figure 17. In these figures it is easily seen that the four curves are qualitatively the same. But there seems to be a discrepancy between Figure 16 and Table 8 because the table asserts that the density variation gives the highest momentum and kinetic energy while the figure shows that the density variation yields a velocity curve that lies below the other two. In fact, from the table, the order of the jets would be density variation, energy variation, and gamma variation while the figure shows just the opposite: gamma, energy, and density. The key to this puzzle lies in the mass going into the jet. The reason for the density variation jet being so much higher in energy and momentum than the gamma variation jet in the table is because the former is much more massive and hence, everything that depends on mass is much higher and the velocity difference is not sufficient to offset the mass difference.

As an application of all this, consider some quantity, J, which characterizes the jet. It is desired to estimate the change in J if some other explosive were substituted for pentolite. First calculate:

$$C_{\rho} = \frac{J\ (\rho_o + 0.1\rho_o) - J\ (\rho_o)}{0.1\rho_o}$$

and then calculate $C\gamma$ and C_Q by similar formulas. Then, approximately:

$$\Delta J = C_\rho \Delta\rho_o + C_\gamma \Delta\gamma + C_Q \Delta Q$$

This will be an estimate of the change in J when ρ_o, γ, and Q are changed by $\Delta\rho_o$, $\Delta\gamma$, and ΔQ, respectively. As an example, we take the experimentally measured jet tip velocities measured by Simon[4] for the BRL precision shaped charge. First, we need the calculated jet tip velocities using the four simulated explosives:

Table 9

Jet Tip Velocity vs. Time for All Four Explosives

	Tip Velocity (cm/μsec)			
Time	Pentolite	$\Delta\rho$	ΔE	$\Delta\gamma$
10	.36822	.42040	.41063	.39724
20	.76304	.77880	.79239	.79404
30	.81856	.83708	.85218	.85513
40	.83242	.84723	.86376	.87004

These values are plotted in Figure 18 and the curves seem to level off near 40 μseconds. Hence, the 40 μsecond value is chosen as the tip velocity. We can now calculate our coefficients:

$$C_\gamma = \frac{v\ (\gamma+.1\gamma) - v(\gamma)}{.1\gamma} = .13532$$

Similarly, $C_Q = 6.46186$ and $C_\rho = .08975$. The results of Simon are summarized in Table 10. His values of detonation pressure, detonation velocity, and loading density (columns 2, 3, and 4 of Table 10) lead to different values of gamma and energy (columns 5 and 6 of Table 10) for pentolite than those used in the calculations. But his values are used for consistency's sake. Column 1 contains the name of the explosive used; columns 2, 3, and 4 contain estimated values of the detonation pressure, detonation velocity, and density supplied by the installation that loaded the explosives. Columns 5 and 6 contain the values of γ and Q calculated from columns 2, 3, and 4. Columns 7, 8, and 9 contain the difference between the values of ρ_o, γ, and Q for the explosive of column 1 and the values for pentolite. Column 9 contains the change in value of jet tip velocity from pentolite as calculated by the method outlined above, and column 11 contains the change in jet tip velocity as measured by Simon. Column 12 has the percentage difference between columns 10 and 11. Although the

Table 10

Variation of Jet Tip Velocity with Explosive Parameters

Explosive	p(mbars)	D(cm/μsec)	ρ gm/cc	γ	Q	Δρ	Δγ	ΔQ	Δv(calc)	Δv(meas)	%
PBXW-111	.35	.88	1.813	3.011	.0480	.163	-.024	.0137	.0999	.106	6
Octol 75/25	.32	.86	1.810	3.183	.0405	.160	.148	.0062	.0745	.104	28
PBXW-110	.32	.85	1.763	2.981	.0458	.113	-.054	.0015	.0771	.104	26
Octol 70/30	.31	.83	1.800	3.000	.0431	.150	-.035	.0088	.0656	.065	1
Comp B	.27	.79	1.680	2.883	.0426	.030	-.152	.0083	.0358	.028	28
TNT	.19	.68	1.640	2.991	.0291	-.010	-.044	-.0052	-.0405	-.063	38
Pentolite	.23	.75	1.650	3.035	.0343						

percentage difference may be as great as 38%, some of them are rather small and only once does a difference greater than 28% appear. This is fairly good when allowance is made not merely for the usual experimental errors involved in measurement of so complex a phenomenon but also for the fact that the coefficients were calculated for a substantially different liner than the one used in the experiments. Furthermore, slight errors in columns 2, 3, and 4 lead to relatively large errors in columns 8, 9, and 10. All things considered, the agreement is remarkably good.

CONCLUSIONS

We can conclude that the method of estimating variations in shaped charge performance by using the calculated coefficients seems to work and merits further study.

We can also conclude, all other things being equal (which rarely happens), that the best shaped charge explosive is the densest.

We can also conclude that point initiation is a poor initiation system and that the circumferential initiation seems to be the best and merits further study.

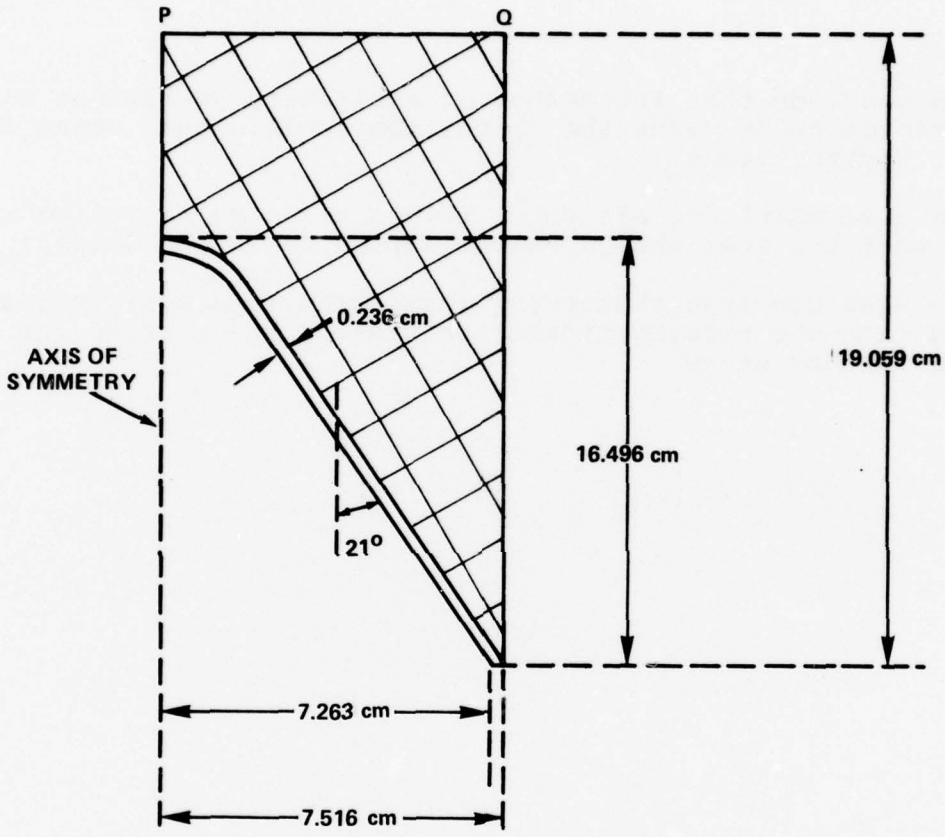

FIG. 1 CROSS SECTION OF THE 42° CONE, SHOWING THE DIMENSIONS

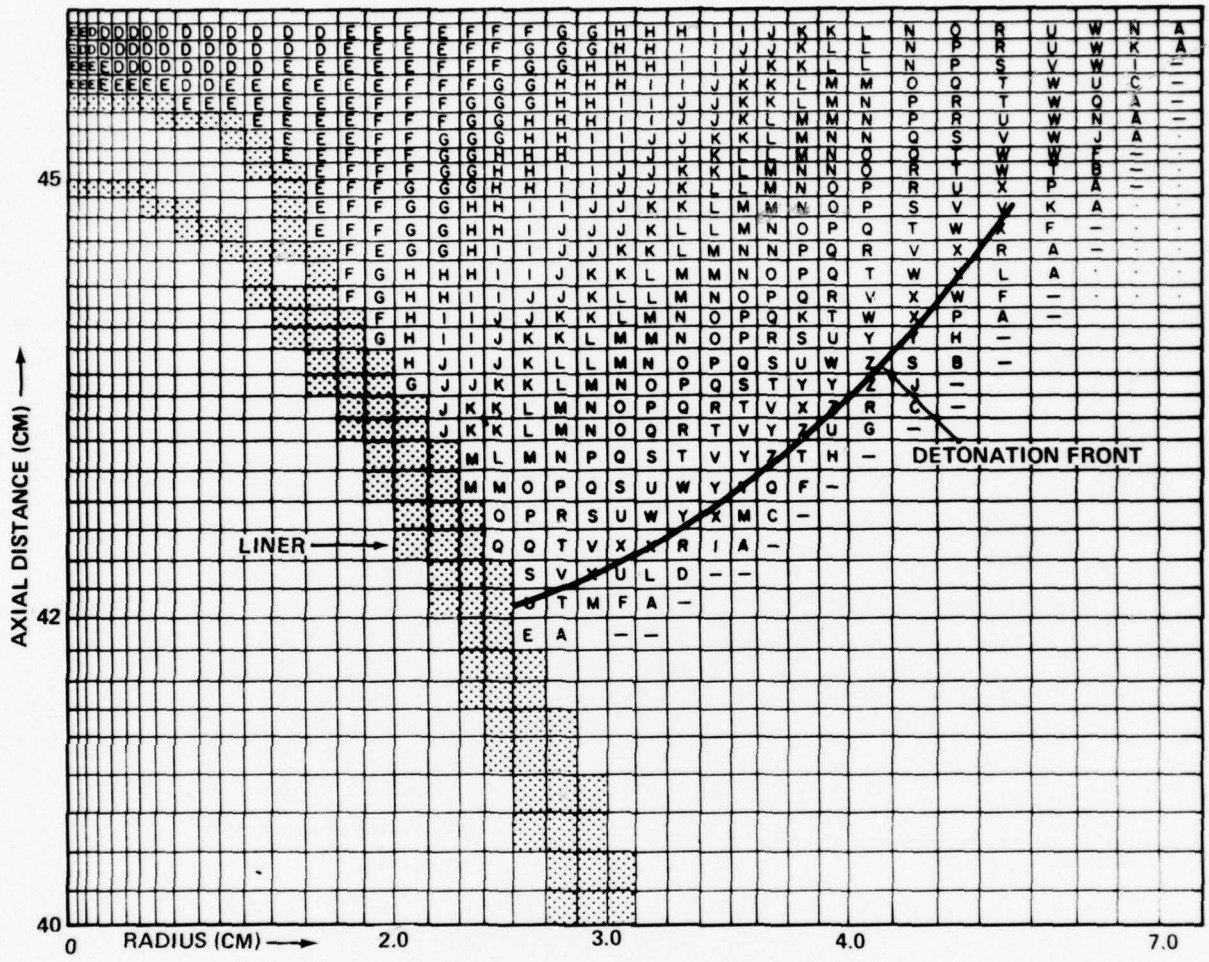

PRESSURE RANGES (dynes/sq. cm)

–	0.	9.06×10^{8}	I	7.25×10^{10}	8.15×10^{10}	R	1.54×10^{11}	1.63×10^{11}
A	9.06×10^{8}	9.06×10^{9}	J	8.15×10^{10}	9.06×10^{10}	S	1.63×10^{11}	1.72×10^{11}
B	9.06×10^{9}	1.81×10^{10}	K	9.06×10^{10}	9.96×10^{10}	T	1.72×10^{11}	1.81×10^{11}
C	1.81×10^{10}	2.72×10^{10}	L	9.96×10^{10}	1.09×10^{11}	U	1.81×10^{11}	1.90×10^{11}
D	2.72×10^{10}	3.62×10^{10}	M	1.09×10^{11}	1.18×10^{11}	V	1.90×10^{11}	1.99×10^{11}
E	3.62×10^{10}	4.53×10^{10}	N	1.18×10^{11}	1.27×10^{11}	W	1.99×10^{11}	2.08×10^{11}
F	4.53×10^{10}	5.43×10^{10}	O	1.27×10^{11}	1.36×10^{11}	X	2.08×10^{11}	2.17×10^{11}
G	5.43×10^{10}	6.43×10^{10}	P	1.36×10^{11}	1.45×10^{11}	Y	2.17×10^{11}	2.26×10^{11}
H	6.43×10^{10}	7.25×10^{10}	Q	1.45×10^{11}	1.54×10^{11}	Z	2.26×10^{11}	2.35×10^{11}

FIG. 2 PRESSURE MAP FOR POINT INITIATED MODE, 10μ SEC

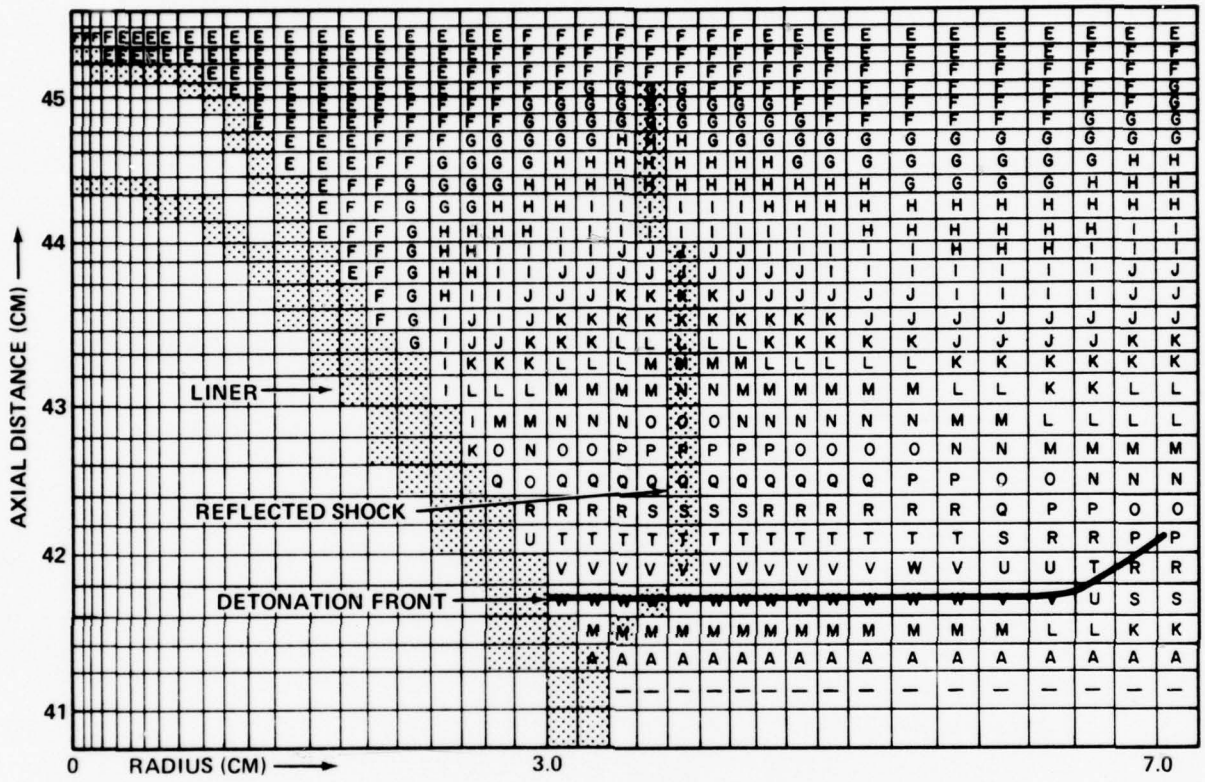

PRESSURE RANGES (dynes/sq. cm)

-	0. - 1.24×10^{9}	I	9.93×10^{10} - 1.12×10^{11}	R	2.11×10^{11} - 2.23×10^{11}
A	1.24×10^{9} - 1.24×10^{10}	J	1.12×10^{10} - 1.24×10^{11}	S	2.23×10^{11} - 2.36×10^{11}
B	1.24×10^{10} - 2.48×10^{10}	K	1.24×10^{11} - 1.37×10^{11}	T	2.36×10^{11} - 2.48×10^{11}
C	2.48×10^{10} - 3.72×10^{10}	L	1.37×10^{11} - 1.49×10^{11}	U	2.48×10^{11} - 2.61×10^{11}
D	3.72×10^{10} - 4.97×10^{10}	M	1.49×10^{11} - 1.61×10^{11}	V	2.61×10^{11} - 2.73×10^{11}
E	4.97×10^{10} - 6.21×10^{10}	N	1.61×10^{11} - 1.74×10^{11}	W	2.73×10^{11} - 2.86×10^{11}
F	6.21×10^{10} - 7.45×10^{10}	O	1.74×10^{11} - 1.86×10^{11}	X	2.86×10^{11} - 2.98×10^{11}
G	7.45×10^{10} - 8.69×10^{10}	P	1.86×10^{11} - 1.99×10^{11}	Y	2.98×10^{11} - 3.10×10^{11}
H	8.69×10^{10} - 9.93×10^{10}	Q	1.99×10^{11} - 2.11×10^{11}	Z	3.10×10^{11} - 3.23×10^{11}

FIG. 3 PRESSURE MAP FOR PLANE WAVE INITIATED MODE, 10μSEC

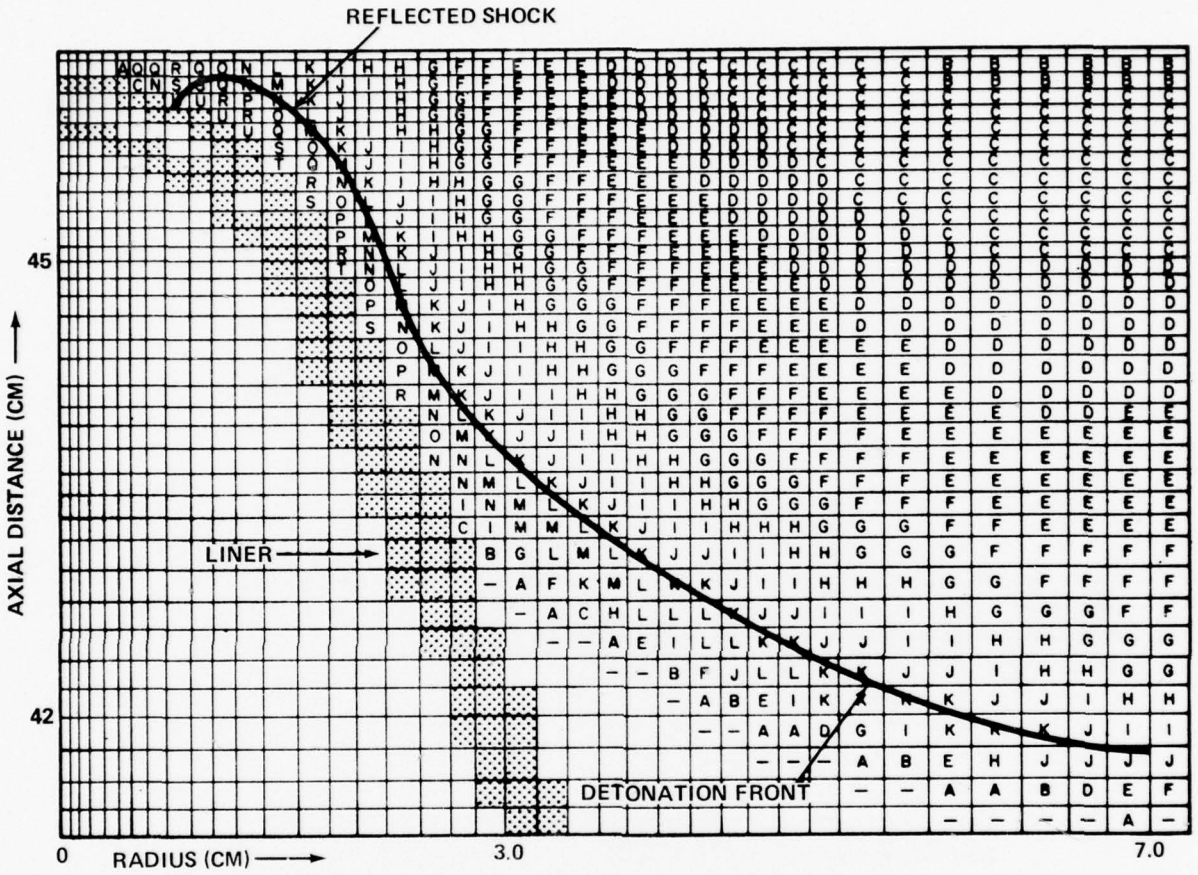

PRESSURE RANGES (dynes/sq. cm)

–	0.	- 2.27×10^{9}	I	1.81×10^{11}	- 2.04×10^{11}	R	3.85×10^{11}	- 4.08×10^{11}
A	2.27×10^{9}	- 2.27×10^{10}	J	2.04×10^{11}	- 2.27×10^{11}	S	4.08×10^{11}	- 4.31×10^{11}
B	2.27×10^{10}	- 4.53×10^{10}	K	2.27×10^{11}	- 2.49×10^{11}	T	4.31×10^{11}	- 4.53×10^{11}
C	4.53×10^{10}	- 6.80×10^{10}	L	2.49×10^{11}	- 2.72×10^{11}	U	4.53×10^{11}	- 4.76×10^{11}
D	6.80×10^{10}	- 9.07×10^{10}	M	2.72×10^{11}	- 2.95×10^{11}	V	4.76×10^{11}	- 4.99×10^{11}
E	9.07×10^{10}	- 1.13×10^{11}	N	2.95×10^{11}	- 3.17×10^{11}	W	4.99×10^{11}	- 5.21×10^{11}
F	1.13×10^{11}	- 1.36×10^{11}	O	3.17×10^{11}	- 3.40×10^{11}	X	5.21×10^{11}	- 5.44×10^{11}
G	1.36×10^{11}	- 1.59×10^{11}	P	3.40×10^{11}	- 3.63×10^{11}	Y	5.44×10^{11}	- 5.67×10^{11}
H	1.59×10^{11}	- 1.81×10^{11}	Q	3.63×10^{11}	- 3.85×10^{11}	Z	5.67×10^{11}	- 5.89×10^{11}

FIG. 4 PRESSURE MAP FOR THE CIRCUMFERENTIALLY INITIATED MODE, 10μSEC

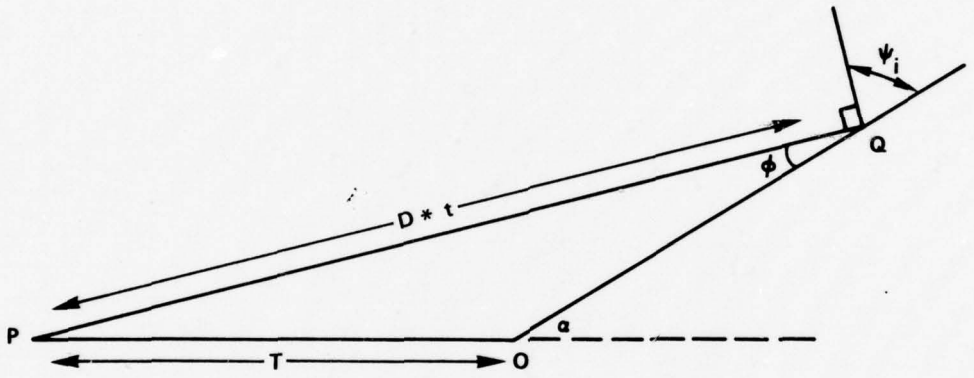

FIG. 5 ANGLE OF INCIDENCE OF THE DETONATION WAVE ON THE LINER FOR THE POINT DETONATED MODE

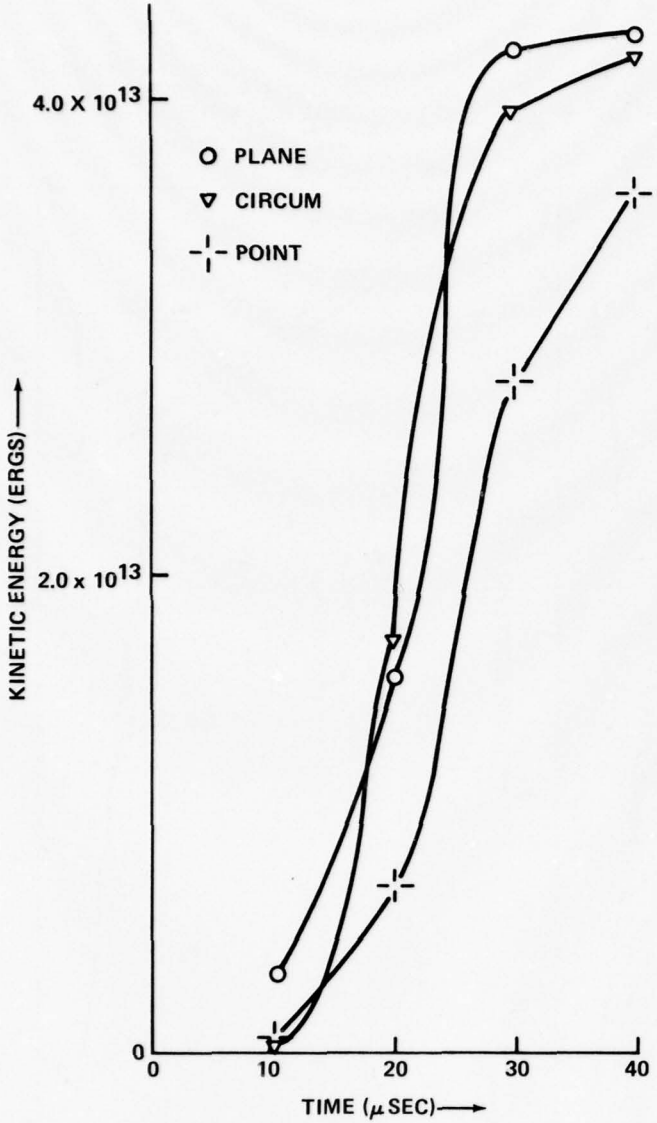

FIG. 6 TOTAL KINETIC ENERGY OF THE METAL VS TIME FOR THE THREE MODES OF INITIATION

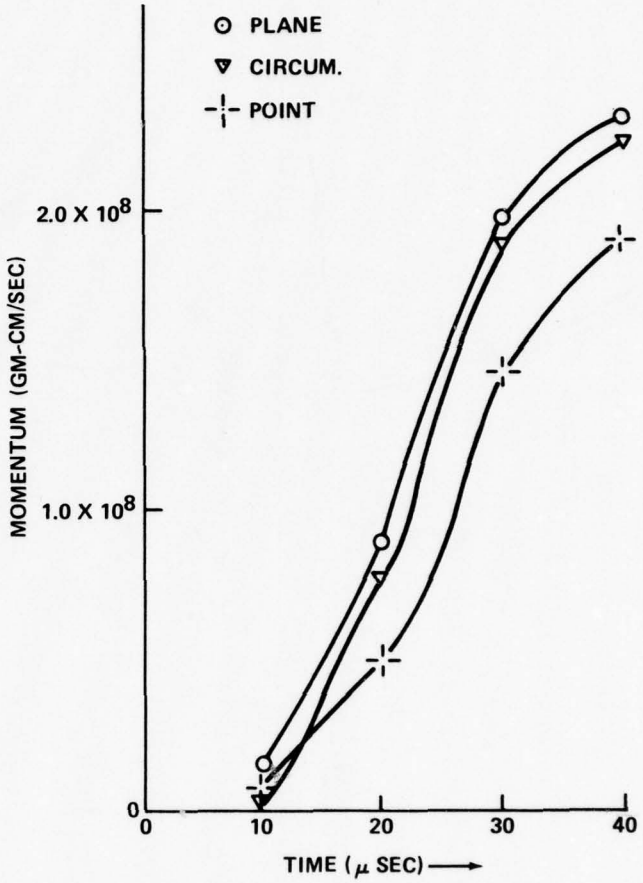

FIG. 7 TOTAL MOMENTUM OF THE METAL VS TIME FOR THE THREE MODES OF INITIATION

NOTE: ALL AXIAL DISTANCES MEASURED FROM THE BOTTOM OF THE COMPUTATIONAL GRID.

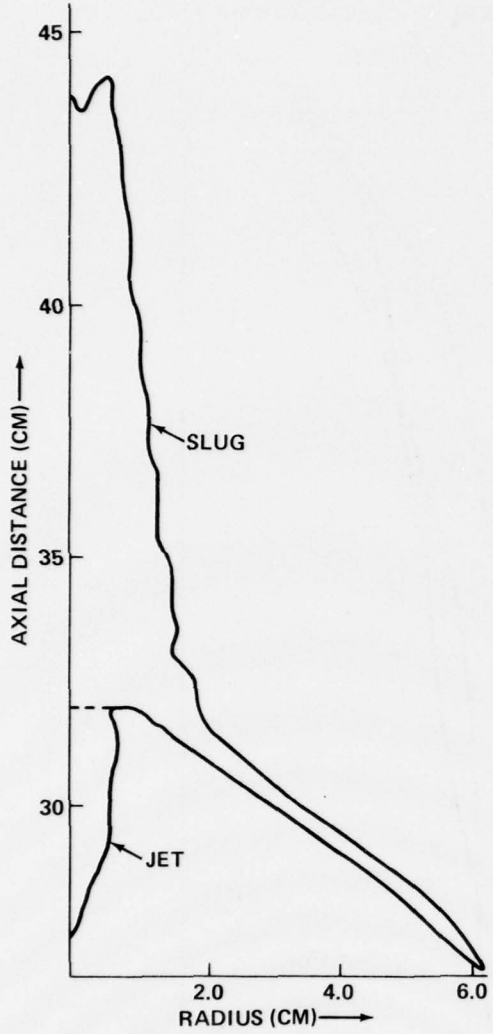

FIG. 8 LINER POSITION FOR THE 42 DEGREE CONE, POINT INITIATED MODE, 40μ SEC

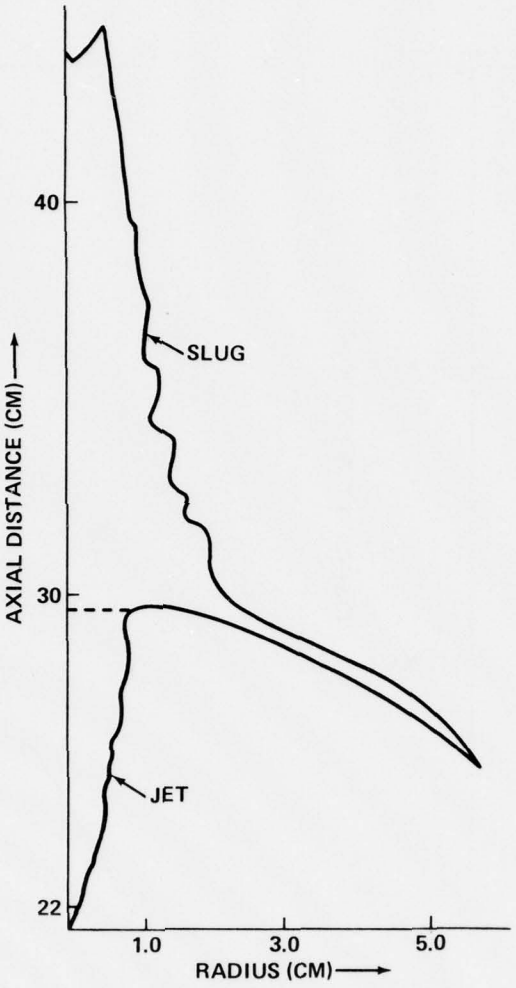

FIG. 9 LINER POSITION FOR THE 42 DEGREE CONE, PLANE INITIATED MODE, 40μ SEC

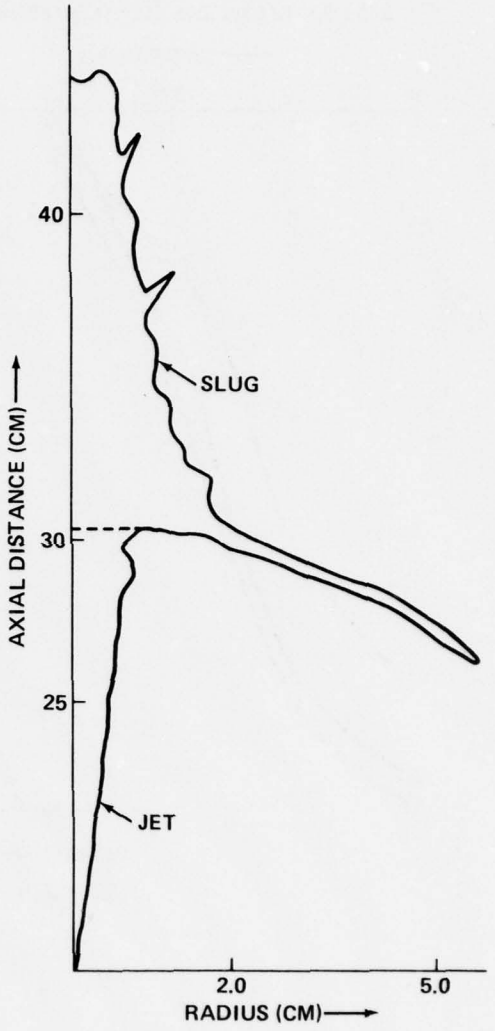

FIG. 10 LINER POSITION FOR THE 42 DEGREE CONE, CIRCUMFERENTIALLY INITIATED MODE, 40μ SEC

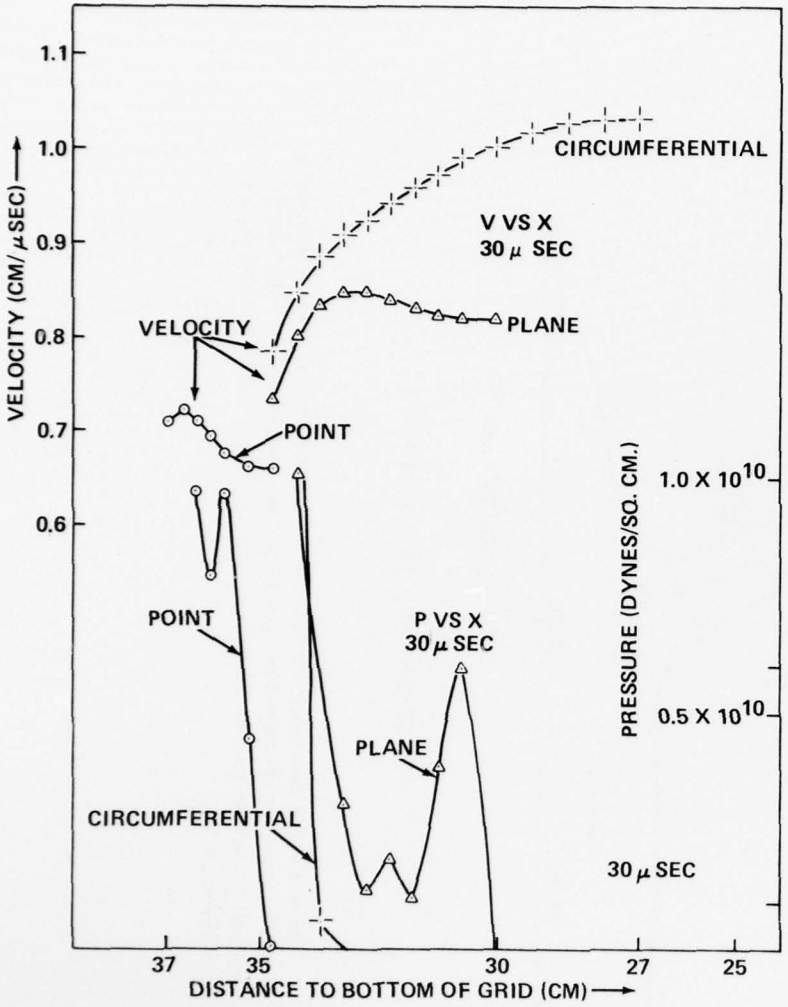

FIG. 11 VELOCITY AND PRESSURE IN THE JET AT 30 μ SEC FOR ALL THREE MODES OF INITIATION

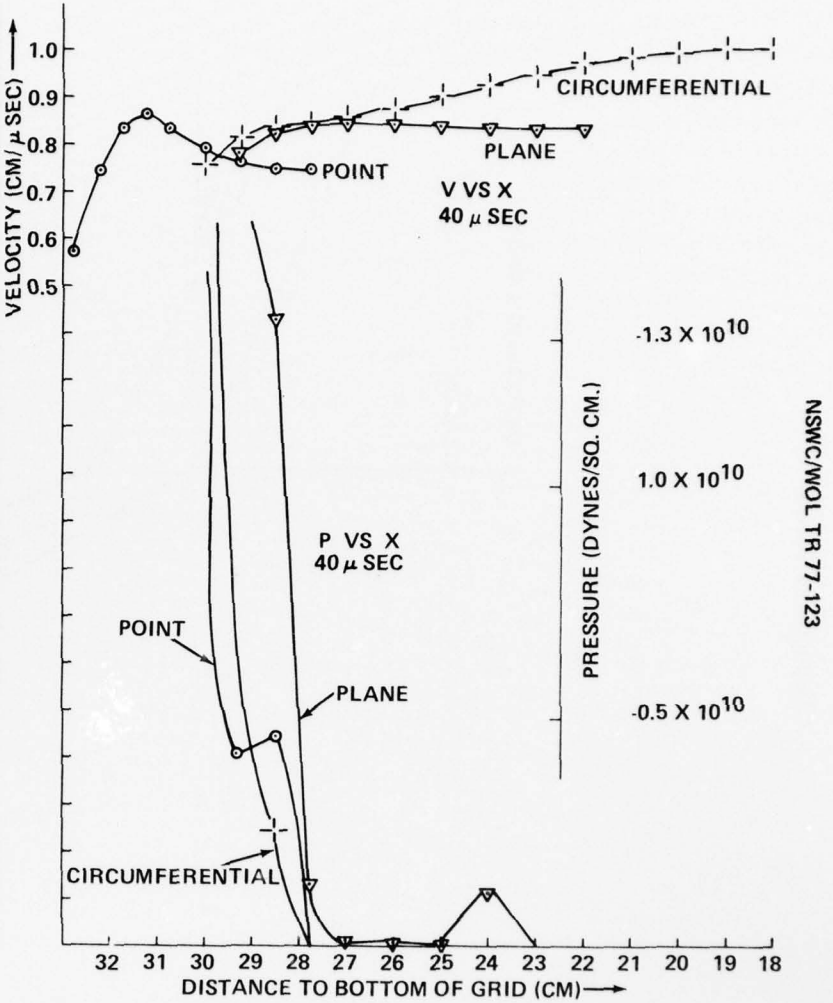

FIG. 12 VELOCITY AND PRESSURE IN THE JET AT 40 μ SEC (ALL 3 MODES OF INITIATION)

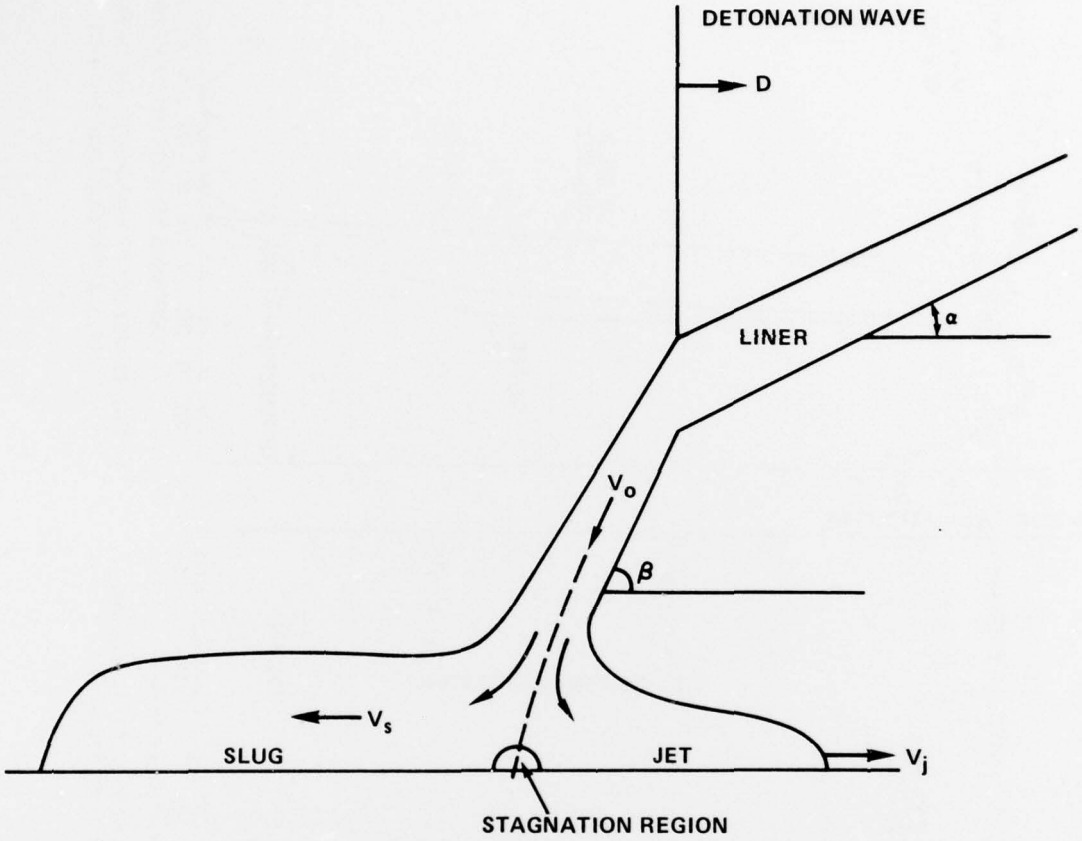

FIG. 13 COLLAPSE OF THE LINER

The detonation wave bends the liner and drives it inward. The velocity with which the material flows into the stagnation region is V_o, the collapse velocity. The velocity with which it flows out towards the jet is V_j and the velocity with which it flows out toward the slug is V_s.

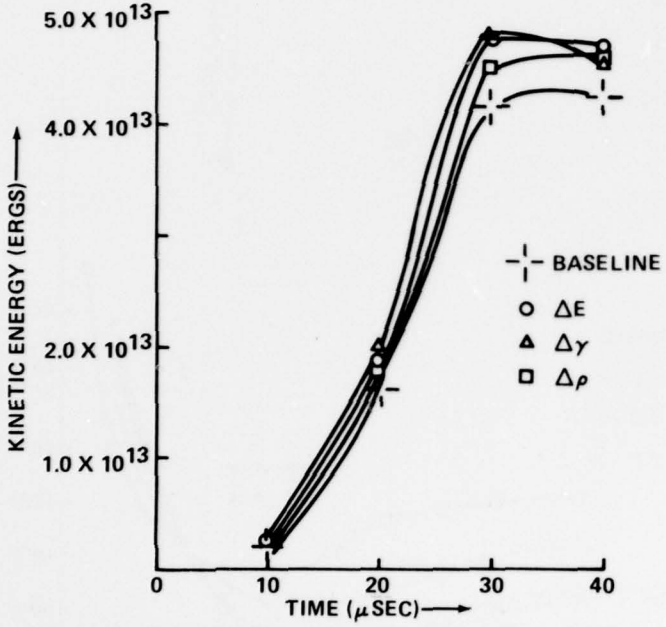

FIG. 14 TOTAL KINETIC ENERGY IN THE METAL VS TIME FOR FOUR EXPLOSIVES

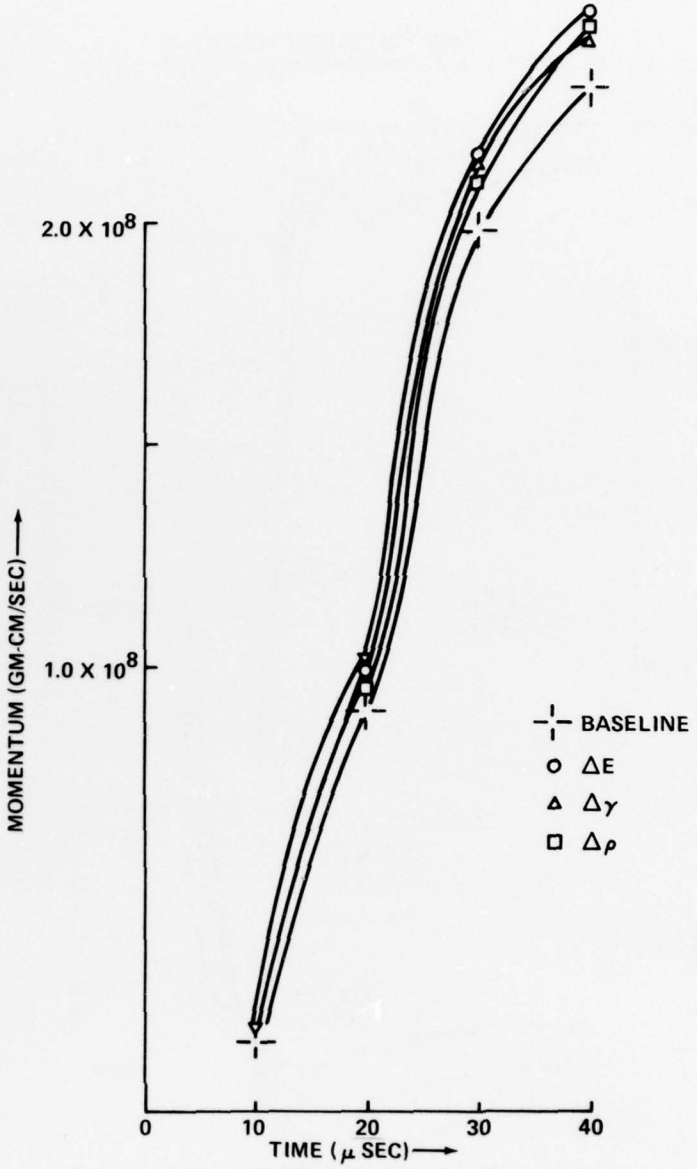

FIG. 15 TOTAL MOMENTUM IN THE METAL VS TIME FOR FOUR EXPLOSIVES

NOTE : ALL AXIAL DISTANCES MEASURED FROM THE BOTTOM OF THE COMPUTATIONAL GRID. (CM)

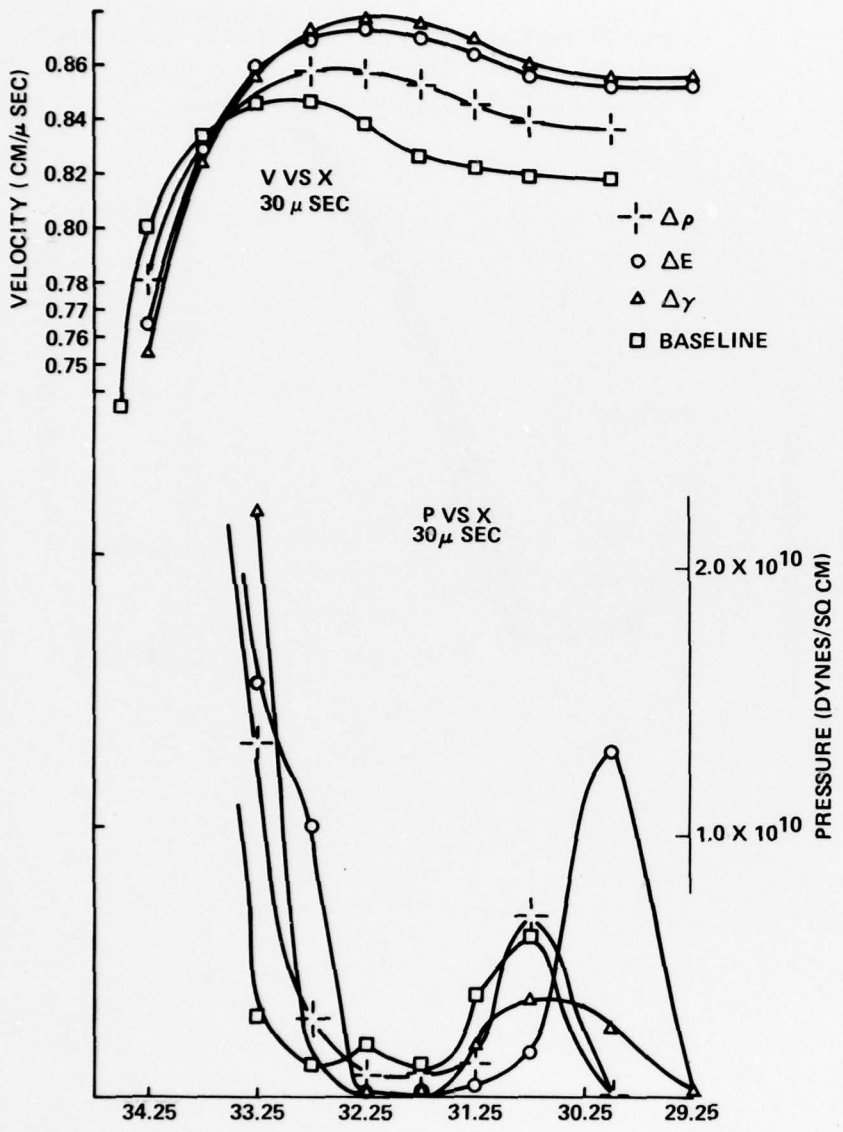

FIG. 16 VELOCITY AND PRESSURE IN THE JET VS DISTANCE FOR FOUR EXPLOSIVES (30 μ SEC)

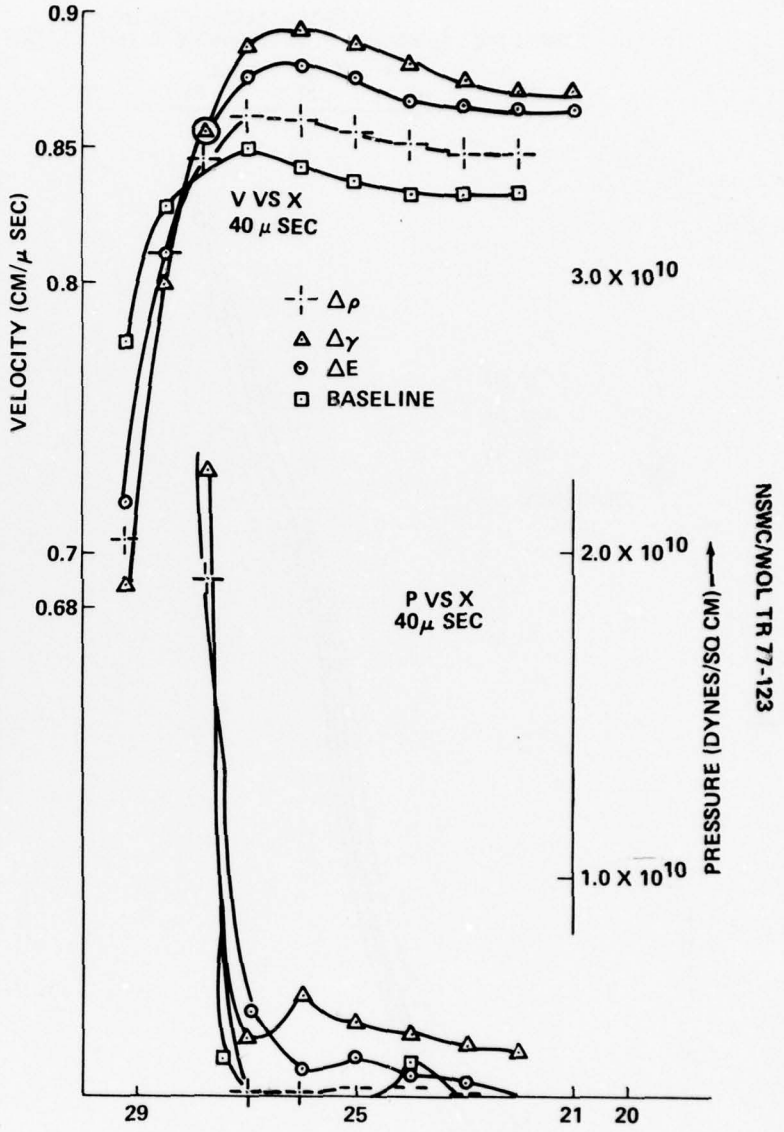

FIG. 17 VELOCITY AND PRESSURE IN THE JET VS DISTANCE FOR FOUR EXPLOSIVES (40 μ SEC)

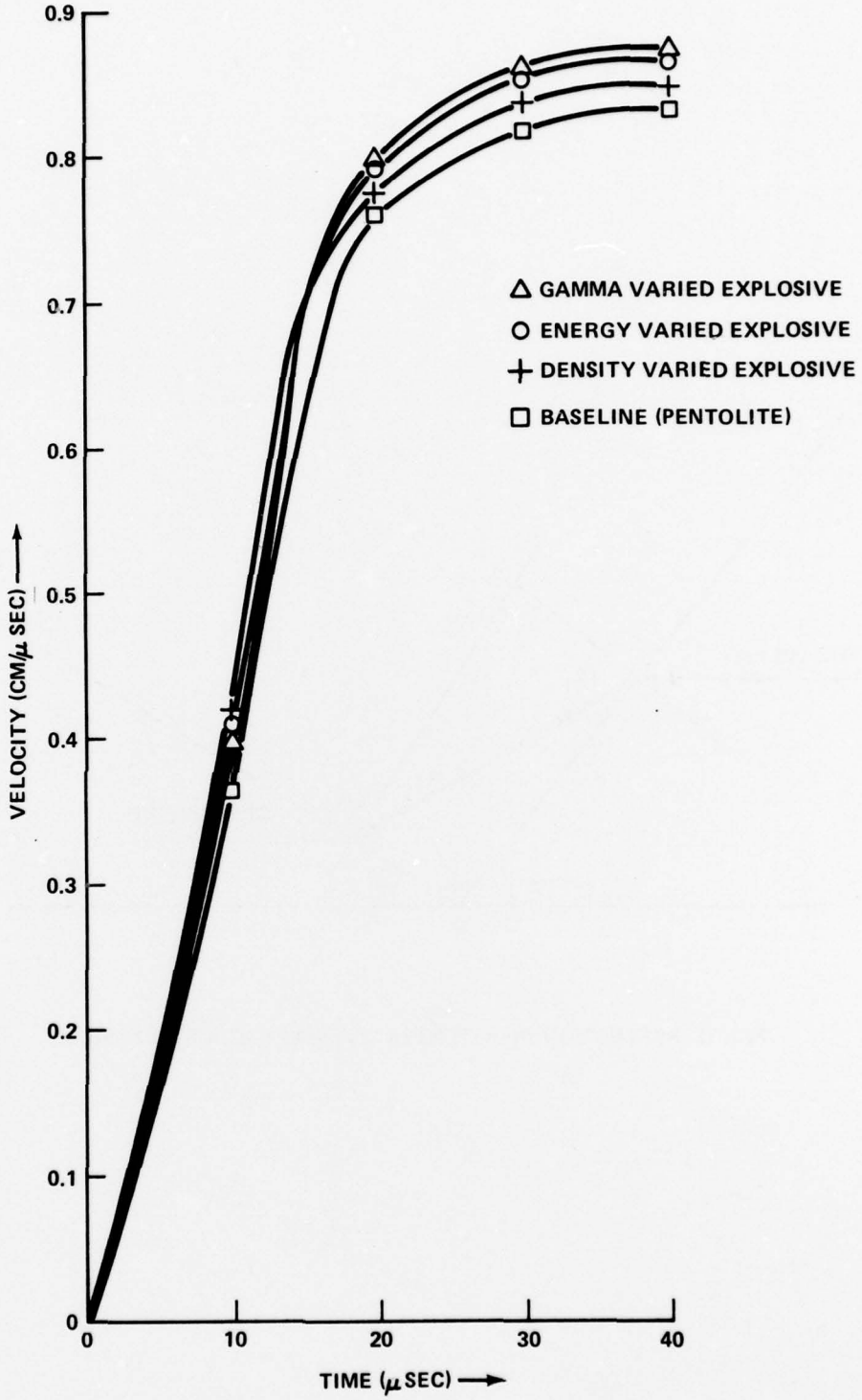

FIG. 18 JET TIP VELOCITY VS TIME (ALL FOUR EXPLOSIVES)

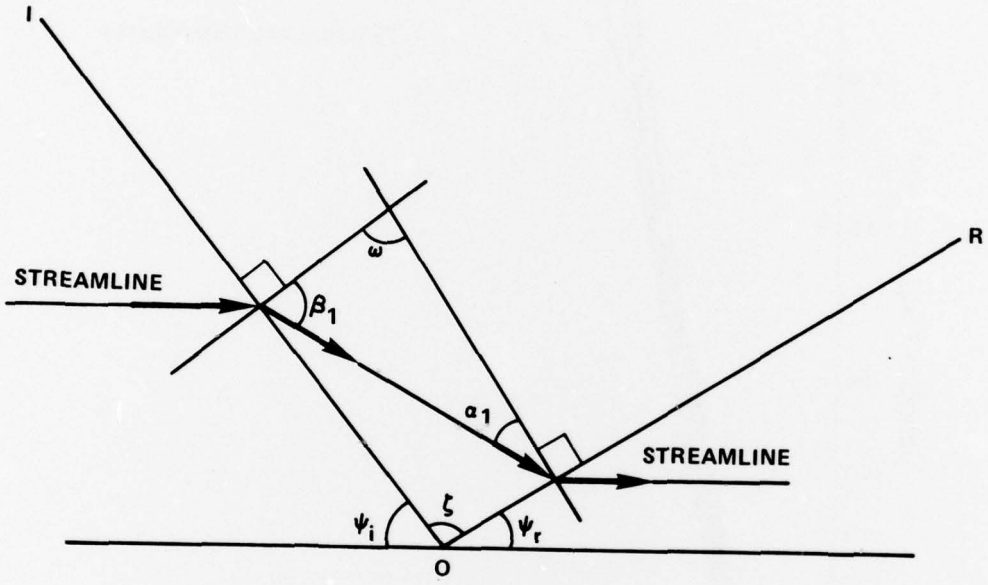

FIG. 19 REFLECTION OF A DETONATION WAVE AT A RIGID WALL

REFERENCES

1. Gittings, M. L., BRLSC: An Advanced Eulerian Code for Predicting Shaped Charges, BRL Contract Report No. 279, 1975.

2. P. Chou, J. Carleone, and R. Karpp, Journal of Applied Physics, 47, 1976, p. 2975.

3. G. Birkhoff, D. MacDougall, E. Pugh, and G. I. Taylor, Journal of Applied Physics, 19, 1948, p. 563.

4. Simon, J., The Effects of Explosive Detonation Characteristics on Shaped Charge Performance, BRL Memorandum Report 2414.

5. Dunn, B., "Mach Reflection of Detonation Waves in High Explosives, II," Physics of Fluids, 7, 1964, p. 1707.

Appendix A

Suppose a detonation wave is incident upon a rigid wall. A shock wave appears at the intersection of the wall and the detonation wave. This shock is called the reflected shock wave. We wish to determine the angle between the reflected shock and the wall. The geometry is as shown in Figure 19. The angles, ψ_i and ψ_r are the angles of incidence and reflection, respectively. The flow is from left to right and, in the coordinate system chosen (with the point, O, at rest), the material moves into the detonation wave with a velocity, $D \csc(\psi_i)$. It emerges from the detonation wave with a velocity, q_1, which makes an angle, β_1, with the normal to the detonation front.* The pressure, density and energy of the flow, as it emerges from the detonation front, are the Chapman-Jouguet values. The flow is incident upon the reflected shock at an angle, α_1, to the normal. We seek the angle of reflection, ψ_r, and this can be obtained from the angle, α_1, through the following reasoning:

From Figure 19,

$$\omega + \beta_1 + \alpha_1 = \pi$$

$$\omega + \pi/2 + \zeta + \pi/2 = 2\pi$$

$$\zeta + \psi_i + \psi_r = \pi$$

Hence:

$$\psi_i + \psi_r + \beta_1 + \alpha_1 = \pi$$

Therefore

$$\tan \psi_r = -\tan(\psi_i + \alpha_1 + \beta_1)$$

$$= -\frac{\tan(\psi_i + \beta_1) + \tan \alpha_1}{1 + \tan(\psi_i + \beta_1)\tan \alpha_1}$$

*The heavy arrows in Figure 19 indicate the streamlines in a coordinate system fixed with respect to the point, O.

Using the work of Dunne [5],

$$\tan \beta_1 = \frac{\gamma + 1}{\gamma} \cot \psi_i$$

(formula 8, op. cit.) and hence

$$\tan(\psi_i + \beta_1) = \frac{(\gamma + 1) + \gamma \tan^2 \psi_i}{(2\gamma + 1) \tan \psi_i}$$

When ψ_i and γ are given, this expression is known and the tangent of the angle of reflection can be computed by the earlier formula as soon as α_1 is known. To compute α_1 we employ formula 23 of Dunne's work [5]:

$$\frac{\gamma \cot \alpha_1 \tan^2 \psi_i + (\gamma + 1) \cot \alpha_1 - \tan \psi_i}{\cot \alpha_1 \left[\gamma \tan^2 \psi_i + (\gamma + 1) + \cot \alpha_1 \tan \psi_i\right]}$$

$$- \frac{2\gamma^2}{(\gamma + 1) \cos^2 \alpha_1 \left[\gamma^2 + (\gamma + 1)^2 \cot^2 \psi_i\right]}$$

$$- \frac{\gamma - 1}{\gamma + 1} = 0$$

This is an equation for $\cot \alpha_1$ with ψ_i and γ as parameters. By clearing the fractions and grouping powers of $\cot \alpha_1$ together, we obtain:

$$\cot^3 \alpha_1 \left\{2\gamma^2 + (\gamma - 1)(\gamma^2 + (\gamma + 1)^2 \cot^2 \psi_i)\right\} \tan \psi_i$$

$$- \cot^2 \alpha_1 \left\{2(\gamma + 1)^2 \cot^2 \psi_i \, (\gamma \tan^2 \psi_i + \gamma + 1)\right\}$$

$$+ \cot \alpha_1 \left\{(\gamma + 1)^3 \cot^2 \psi_i + \gamma^2 (\gamma + 3)\right\} \tan \psi_i$$

$$+ 2\gamma^2 (\gamma \tan^2 \psi_i + \gamma + 1) = 0$$

This is a cubic equation for $\cot \alpha_1$. Since $0 < \alpha_1 < 1/2\,\pi$, the possible values of α_1 are positive real numbers. Examining the coefficients of the equation, we see that the coefficient of $\cot^2 \alpha_1$ is negative and all the other coefficients are positive. By Descartes' Law of Signs, the number of positive real roots is either 2 or 0. It is easily shown that there is exactly 1 negative real root and we are left with the well known result: that either there are two possible reflections (the strong and the weak reflections) or there is no possible regular reflection. In the latter case, the roots are imaginary.

To determine the nature of the reflection in our cases, we consider first the point detonated explosive. Here, $\psi_i = 82.8^\circ$ and $\gamma = 2.78$. Using the standard algorithm for solving cubic equations:

$$\psi_i = 82.831^\circ \qquad \gamma = 2.78$$

$$\left.\begin{aligned} a &= 235.4582114 \\ b &= -81.15242593 \\ c &= 361.9410554 \\ d &= 2774.5337962 \end{aligned}\right\} \text{ coefficients}$$

$$z = y - b/3a; \quad z^3 + 3Hz + G = 0 \qquad \text{reduced equation}$$

$$H = .4991937361$$

$$G = 11.95713568$$

$$u^3 = 1/2(-G + \sqrt{G^2 + 4H^3}) = .010394482$$

$$u = .2182399723$$

$$v = -H/u = -2.287361695$$

$$Z_1 = u + v = -2.06912173$$

$$2Z_2 = -(u + v) + (u - v)\sqrt{3}\, i$$

$$2Z_3 = -(u + v) - (u - v)\sqrt{3}\, i$$

Z_2 and Z_3 are complex and Z_1 is negative. The corresponding values of cot α are also either complex or negative and there is no genuine solution to the regular reflection problem. The reflection must be a Mach reflection. The plane wave initiated problem is solved similarly. Here $\psi_i = 48^\circ$ and $\gamma = 2.78$ (as above).

$$\psi_i = 48^\circ \qquad \gamma = 2.78$$

$$\left.\begin{aligned} a &= 55.34500733 \\ b &= -167.0185289 \\ c &= 98.24218914 \\ d &= 111.4283686 \end{aligned}\right\} \text{ coefficients}$$

$Z = y - b/3a \qquad Z^3 + 3HZ + G = 0$ (reduced cubic)

$$G = 1.763190504$$

$$H = -.4201864861$$

$$u^3 = 1/2(-G + \sqrt{G^2 + 4H^3}) = -.0431303117$$

$$u = -.3506933513$$

$$v = -H/u = -1.198159259$$

$$Z_1 = u + v = -1.548852611$$

$$2Z_2 = 1.548852611 + .8474659077i$$

$$2Z_3 = 1.548852611 - .8474659077i$$

As in the previous case, all the roots of the reduced cubic are either negative or imaginary. The corresponding values of cot α_i are also negative or imaginary and there is no genuine solution to the reflection problem. The reflection must be an irregular, Mach reflection.

DISTRIBUTION LIST

Commander
Ballistics Research Laboratory
Alberdeen Proving Ground, MD 21005
(Dr. F. I. Grace)
(Dr. A. Dietrich)
(Mr. J. Harrison)
(Mr. B. Scott)

Commander
ARRADCOM
Dover, NJ 07801
(Mr. G. Randers-Pehrson)
(Dr. J. Pearson)

Science, Systems and Software Corp.
P. O. Box 1620
La Jolla, CA 92037
(Mr. Sedgwick)

Commander
Naval Sea Systems Command
Washington, D. C. 20362
(PMS406)
(PMS406E)
(PMS406E3)
(SEA0333)

Commander
Naval Ocean Systems Command
San Diego, CA 92152
(F. Marshall, Code 0609)
(ALWT Library Code 4473-B)

Army Mobility Equipment Research and Development Center
Fort Belvoir, VA 22060
(J. W. Bond)

Distribution List (Cont.)

Commander
Naval Weapons Center
China Lake, CA 93555

Defense Documentation Center
Cameron Station
Alexandria, Virginia 22314 12

NDW-NSWC(W)-5605/1 (Rev. 5-78)

TO AID IN UPDATING THE DISTRIBUTION LIST FOR NAVAL SURFACE WEAPONS CENTER, WHITE OAK TECHNICAL REPORTS PLEASE COMPLETE THE FORM BELOW:

TO ALL HOLDERS OF NSWC/WOL/TR 77-123
by J. P. Coughlin, Code R-13

DO NOT RETURN THIS FORM IF ALL INFORMATION IS CURRENT

A. FACILITY NAME AND ADDRESS *(OLD) (Show Zip Code)*

NEW ADDRESS *(Show Zip Code)*

B. ATTENTION LINE ADDRESSES:

C.

☐ REMOVE THIS FACILITY FROM THE DISTRIBUTION LIST FOR TECHNICAL REPORTS ON THIS SUBJECT.

D.
NUMBER OF COPIES DESIRED _____

GPO 930-764

DEPARTMENT OF THE NAVY
NAVAL SURFACE WEAPONS CENTER
WHITE OAK, SILVER SPRING, MD. 20910

OFFICIAL BUSINESS
PENALTY FOR PRIVATE USE, $300

POSTAGE AND FEES PAID
DEPARTMENT OF THE NAVY
DOD 316

U.S.MAIL

COMMANDER
NAVAL SURFACE WEAPONS CENTER
WHITE OAK, SILVER SPRING, MARYLAND 20910

ATTENTION: CODE R-13